Accepted Manuscript

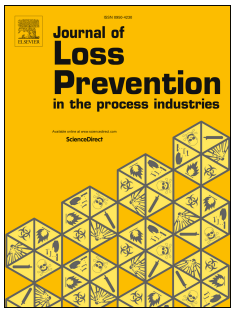

Internal and external pressure prediction of vented gas explosion in large rooms by using analytical and CFD methods

Jingde Li, Hong Hao

PII: S0950-4230(17)30293-0

DOI: 10.1016/j.jlp.2017.08.002

Reference: JLPP 3566

To appear in: *Journal of Loss Prevention in the Process Industries*

Received Date: 25 March 2017

Revised Date: 4 July 2017

Accepted Date: 2 August 2017

Please cite this article as: Li, J., Hao, H., Internal and external pressure prediction of vented gas explosion in large rooms by using analytical and CFD methods, *Journal of Loss Prevention in the Process Industries* (2017), doi: 10.1016/j.jlp.2017.08.002.

Internal and external pressure prediction of vented gas explosion in large rooms by using analytical and CFD methods

Jingde Li[1, a], Hong Hao[1, b]

[1]Center for Infrastructure monitoring and protection, school of Civil and Mechanical Engineering, Curtin University, Kent St, Bentley WA 6102, Australia

[a]jingde.li@curtin.edu.au, [b]hong.hao@curtin.edu.au

Abstract

This paper presents an analytical and a numerical method to predict the internal and external pressures from vented gas explosion in a large enclosure. The first peak internal pressure near the venting of enclosure, which is the primary factor related to the external pressure in far field, is predicted by using analytical correlations. The accuracy of the analytical method is verified by using data from a series of experiments with idealized conditions. However, the incapability of external pressure prediction and over-prediction of peak internal pressure are seen in the realistic scenario by using the analytical approach. Therefore computational Fluid Dynamics (CFD) simulations are consequently performed to accurately estimate both the internal and external pressures of vented explosions. A CFD modelling procedure is suggested in this paper to model the turbulent flame inside the enclosure by using FLACS and to calculate the blast wave propagation with low turbulence in free air by using ANSYS Fluent. This combined CFD modelling approach is proven yielding good predictions of internal and external pressures from vented explosions.

Keywords: external gas explosion; internal pressure; far-field pressure; vented gas explosion; CFD; FLACS; ANSYS Fluent

1. Introduction

Recent accidents of oil and gas tank explosions, such as Nigerian gas tank explosion (Daily-News, 2015), Russia's Far East oil depot explosion (TNA, 2011) and the USA Kansas City's gasoline explosion by lightning strike (Firehouse, 2008), remind us the potential of blast loads from vented or confined gas cloud explosion to severely damage and threaten neighbouring structures and people. The blast load/overpressure escalation is due to the hot burnt gas expansion inside the confined enclosure after a flammable gas mixture is ignited, the fast energy discharge from a gas explosion eventually leads to tremendous damage (Tomlin et al., 2015).

In order to protect the enclosures in which the explosion occurs, engineers and researchers have been developing a series of different explosion mitigation methods (Ferrara et al., 2008; Liang and Zeng, 2010; Janes et al., 2014; Mitu et al., 2016). Amongst, explosion venting is one of the most cost efficient protective techniques applied commonly to discharge the high overpressure of burned and unburned gas to mitigate internal explosions (Van Wingerden, 1989). Since early 1970s, numerous analytical models, empirical correlations (Bradley and Mitcheson, 1978; Cooper et al., 1986; Molkov, 1999; Tamanini, 2001) and engineering guidelines (NFPA-68, 2007, 2013) have been developed to estimate the vented explosion pressure. More recent studies have also been extensively conducted to better understand the turbulent flame acceleration and combustion inside the chamber (Chao et al., 2011; Fakandu et al., 2015; Tomlin et al., 2015; Bao et al., 2016; Qi et al., 2016)

However, compared to the studies on internal pressure of vented explosion, combustion outside the enclosure has received little attention, although it could also be destructive to adjacent/far end structures (Palmer and Tonkin, 1980). The external gas explosion can occur simultaneously or earlier before the flame emerges from the enclosure, which eventually increase the peak pressure (Solberg et al., 1980; Schildknecht and Geiger, 1983). Such effect

of external explosion has been studied least, apart from an "ideal" vented gas explosion. Therefore, the basic understanding of the evolution of external explosion is still unsatisfactory (Fan et al., 2005). For example, the influence of external explosion on internal pressure from a 30 m^3 vented explosion enclosure under different experimental conditions was discussed by (Harrison and Eyre, 1987), but only broad trend of the findings was provided. (Palmer and Tonkin, 1980) derived very simple correlations for external pressure estimation of vented explosion based on a series of methane explosion tests, fundamental models of external explosion calculations were however not provided. Further development of these correlations was also conducted, the non-line-of-sight pressure estimated by ellipsoidal blast wave model predicts better external pressure but revision was still required (Forcier and Zalosh, 2000).

More presently, some experimental findings were updated on external explosion research (Fan et al., 2005; Jiang et al., 2005; Qi et al., 2016) to understand the dynamic processes of external explosion evolution. However, these testing vessels were in small scales. For instance, the cylindrical gas tanks of 180mm inner diameter and 300mm height were considered in (Fan et al., 2005; Jiang et al., 2005). Similarly small cuboid vessels of 100×100×200 mm were used in the vented gasoline-air explosions tests (Qi et al., 2016). The correlative pressures due to Helmholtz oscillations and the Taylor instability initiated from internal explosion cannot be well-captured in small-scale tests, let alone the further estimation of external pressures. In order to accurately predict the external pressures in near and far fields from a vented gas explosion, large-scale experiments and numerical simulations are required.

So far, only limited large-scale external explosion experiments (Palmer and Tonkin, 1980; Harrison and Eyre, 1987; Van Wingerden, 1989) have been performed due to the fact of high operation cost and risk. The simple relationships between the external pressure and the

distance provided in these studies could be merely used to estimate far field pressure in a narrow range of conditions (Forcier and Zalosh, 2000). Some other empirical approaches, such as Multi-Energy Method (MEM), was developed to estimate far-field blast-curves resulted from a potential vapour inside enclosure (Van den Berg, 1985). Baker-Strehlow method, which is similar to MEM, also incorporated findings from experiments to provide basic correlations for combustion energy estimation outside the gas source (Baker et al., 2012). However, these empirical approaches have limited abilities to predict the actual explosion source strength in the far field, as they are incapable of taking into consideration direction, congestion and confinement effects (Hansen et al., 2010b).

Alternately, Computation Fluid Dynamics (CFD), which by far is the most detailed approach for quantifying gas explosion, is able to model different scale explosions and consider abovementioned geometrical effects. For example, the widely-recognized CFD tool FLACS, which has been validated against a wide-variety of gas explosion tests (Mercx et al., 1994; Arntzen, 1998; Middha et al., 2009; Hansen et al., 2010a; Bleyer et al., 2012), is expected to yield rationally accurate estimations for explosion source strengths, confinement and congestion effects at various scales. However, the explosion pressures predicted by FLACS are expected to be accurate only inside the congested regions with gas cloud coverage (Ma et al., 2014), while the proper resolution and deflagration or shock wave modelling outside the leading edge of congestion becomes a challenge (Hansen et al., 2010b).

The sharp front of a shock wave will become smeared using standard FLACS simulation procedure. Consequently, under-prediction of the peak pressures will be seen. Such weakness in far-field blast modelling in FLACS was addressed in another work by (Hansen and Johnson, 2015). The new guidelines indicated that the Courant-Friedrich-Levy numbers based on sound velocity and fluid flow velocity of flame (CFLC and CFLV, respectively) should be reduced to result in smaller numerical time steps. In addition, non-reflecting

boundary condition "PLANE_WAVE" must be applied to avoid too high pressure prediction in far-field generated by numerical boundary reflection. However, the determination of CFLC and CFLV is depending on the parameter of DPDX (Middha and Hansen, 2008), which is a normalized spatial pressure gradient across the flame front. The DPDX parameter is capable of indicating when the flame front captures the pressure front, which is the case when Deflagration to Detonation Transition (DDT) occurs (Gexcon, 2015). The DDT-scenarios are normally in large scale geometries with high congestions (Thomas et al., 2013; Tomlin and Johnson, 2013; Johnson et al., 2015), the overpressures are expected to be over 2 bar at the flame front in these strong explosions. The FLACS new guideline (Hansen and Johnson, 2015) is however not applicable for the external pressure estimation of a vented gas explosion in open space (i.e. non DDT scenario), as the external/far field pressure will be too low to render a untrustworthy magnitude of DPDX.

In order to model the external turbulent flame propagation with low flow velocity and low pressure from a vented gas explosion, ANSYS Fluent software (Fluent, 2009) is another alternative. So far, most ANSYS Fluent studies on vented gas explosions were focusing on internal explosion modelling (Di Sarli et al., 2009; Ab Kadir et al., 2016; Luo et al., 2016). Limited publications on external gas explosion simulation by ANSYS Fluent were available. (Tulach et al., 2015) utilized ANSYS Fluent to carry out vented explosion simulation. By using the turbulent model "k-ω SST" and the combustion model "Eddy-Dissipation Concept", good agreement between the modelled external pressures and experimental data was seen. However, only one set of experiment is numerically modeled, the accuracy of such CFD modelling needs further verification.

In this paper, the analytical models have been firstly investigated and utilized to predict the peak pressures inside the enclosure resulted from external explosion (Bauwens et al., 2010). The peak pressures inside the chambers are well calculated by these correlations, while over-

estimation of internal pressures for explosion from enclosures with layered fuel-air mixture were also observed. Therefore, in order to more precisely predict external/far-field pressure in the large rooms, CFD simulation solvers of FLACS and ANSYS Fluent are utilized. Due to the fact that the accuracy of FLACS in estimation of internal pressure, which is generated from a combination of the external explosion, Helmoholtz oscillations, and the Taylor instability, has been verified in the authors' previous experimental study (Li et al., 2017a), the peak pressures are firstly calculated by using FLACS. The blast wave propagation with low turbulence starting from the vent opening is then modelled by using ANSYS Fluent. Satisfactory agreement between CFD estimated pressures in far-field and experimental data (Palmer and Tonkin, 1980) is obtained.

2. Analytical models for peak pressure calculation

According to the definition of vented explosion pressure by (Harrison and Eyre, 1987), the overpressures in far field from a vented gas explosion are generated both by the peak overpressure at the source (e.g. the vented explosion enclosure) and the effective vent area size. By taking the factors of flame propagation, pressure buildup and venting etc. into account, the external explosion influenced peak pressure near venting can be estimated by using simplified analytical models (Bradley and Mitcheson, 1978; Tamanini, 2002; Bauwens et al., 2010).

2.1 Derivation of Analytical model

The analytical correlations derived by (Bauwens et al., 2008; Bauwens et al., 2010) are newly addressed in this study. Assuming the gas is compressed in adiabatic enclosure, ideal gas equation of state for unburned reactants and burned products becomes

148
$$\left(\frac{P_i}{P_o}\right)^{\gamma^{-1}} V = \frac{m_u}{\rho_{uo}} + \frac{m_b}{\rho_{bo}} \tag{1}$$

149
$$\frac{V}{P_o \gamma}\left(\frac{P_i}{P_o}\right)^{\frac{1-\gamma}{\gamma}} \frac{dP_i}{dt} = \frac{1}{\rho_{uo}}\frac{dm_u}{dt} + \frac{1}{\rho_{bo}}\frac{dm_b}{dt} \tag{2}$$

150 where P_i is the pressure inside an enclosure, P_o is the ambient pressure, V is the enclosure
151 volume, m_b and m_u are masses of products and reactants, ρ_b and ρ_u are densities of products
152 and reactants, γ is the effective ratio of specific heats of fuel.

153 In order to simplify the equations above, a density of ρ_v is used to represent the mixture of
154 vented unburned reactants and burned products. Additionally, by balancing the mass
155 variation and loss due to combustion reaction and venting, the equation (2) is then expressed
156 as:

157
$$S_u A_f \frac{(\rho_{uo} - \rho_{bo})}{\rho_{bo}} \frac{\rho_u}{\rho_{uo}} = \frac{\dot{m}_v}{\rho_v} \tag{3}$$

158 where $\dot{m}_v$ is the mass flow rating during venting, A_f is the flame area in the enclosure and S_u is
159 the burning velocity of the gas. Assuming small pressure rises in the beginning of the
160 combustion inside the enclosure (i.e. $\rho_u/\rho_{uo} \approx 1$) and defining the expansion ratio at initial
161 condition as:

162
$$\sigma = \frac{\rho_{uo}}{\rho_{bo}} = \frac{P \cdot M_u R / T_0}{P \cdot M_b R / T_{f,b}} = \frac{M_u T_{f,b}}{M_b T_0} \tag{4}$$

163 where M_u and M_b are the unburned and burned molecular masses of the gas, T_0 is the initial
164 temperature, and $T_{f,b}$ is the adiabatic flame temperature.

165 The equation (3) is then converted to:

$$S_u A_f = \frac{\dot{m}_v}{\rho_v(\sigma - 1)} \tag{5}$$

According to mass approximation during venting (Tamanini, 1993), the mass flow rate can be represented as:

$$\dot{m}_v = A_v \rho_v c_d \sqrt{\frac{RT_v}{2M_v}\gamma(\gamma+1)\frac{P - P_e}{P_{cr} - P_e}} \tag{6}$$

where P_e is the external pressure, P_{cr} is the critical pressure given by $P_{cr} = P_e [(\gamma+1)/2]^{\gamma/(\gamma-1)}$, A_v is the vent area, R is the ideal gas constant, c_d is the discharge coefficient, M_v and T_v are the molecular weight and temperature of the vented gas, respectively. By defining the dimensionless parameter of $G = [(\gamma+1)/2]^{\gamma/(\gamma-1)} - 1$, the maximum pressure inside the enclosure of the vented gas explosion can be derived as:

$$\frac{P_i}{P_o} = \frac{P_e}{P_o}\left[1 + G\left(\frac{S_u A_f (\sigma - 1)}{c_d}\sqrt{\frac{2M_v}{RT_v \cdot \gamma(\gamma+1)}}\right)^2\right] \tag{7}$$

It is seen in the equation (7) that the peak internal pressure P_i is affected by the external pressure P_e, burning velocity S_u and flame area A_f. Increasing one of the parameters results in the increment of peak internal pressure. In order to thoroughly investigate the correlation between the internal pressure and external pressure, the maximum flame area and burning velocity are calculated as shown below:

For far-end ignition away venting, the flame area in the enclosure is assumed as:

$$A_f^{far-end} = 2\pi\left[\frac{\left(L \cdot \frac{H}{2}\right)^{1.6} + \left(L \cdot \frac{W}{2}\right)^{1.6} + \left(\frac{W}{2} \cdot \frac{H}{2}\right)^{1.6}}{3}\right]^{\frac{1}{1.6}} \tag{8}$$

For centre ignition, the flame area is given by

$$A_f^{centre} = 4\pi\left(1.1\cdot\sigma\cdot S_u\cdot t\right)^2 \quad (9)$$

where L is the enclosure length, H and W are the height and width of the enclosure, respectively. Fig. 1(a) illustrates the flame area calculation diagram for the equation (8).

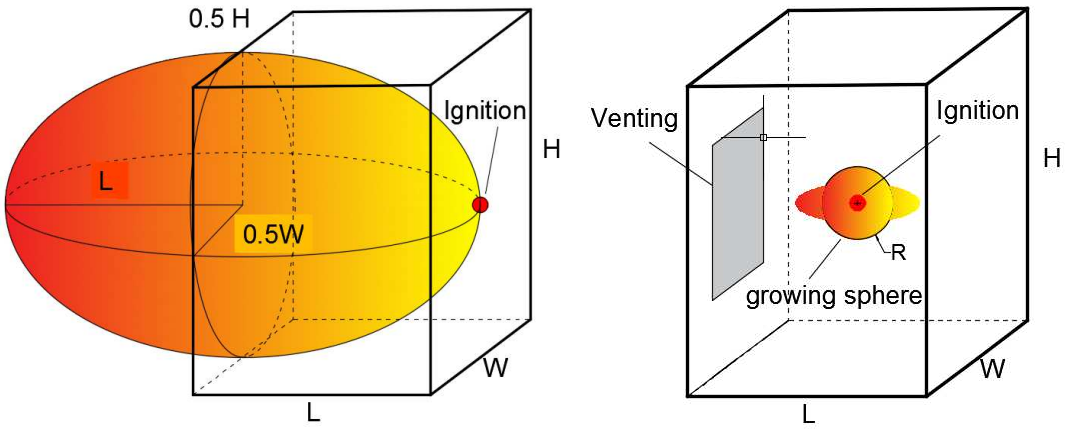

(a) Far-end ignition **(b) Centre ignition**

Fig. 1 Flame area inside the enclosure for the vented explosion

For centre ignition explosion, t in equation (9) is the flame propagation time that flame with a nose tip moving towards to venting (as seen in Fig. 1(b)), and the flame grows with a sphere front initiating from the ignition point with a radius of R. The sphere grows as $R = \sigma\cdot S_u\cdot t$.

194 According to the acoustic approach of (Strehlow, 1979), the peak external pressure due to
195 flame propagation in the gas explosion is given by:

196 $$\frac{P_e}{P_o}-1=\frac{\hat{q}}{4\pi a_0^2 R_e}\frac{d}{dt}\left(S_u(t)A_f(t)\right) \tag{10}$$

197 where a_0 is the velocity of sound in an ideal gas, $\hat{q}$ is an effective dimensionless heat addition,
198 which equals to $\gamma(\rho_u-\rho_b)/\rho_b=\gamma(\sigma-1)$. R_e is the radius of the flame volume in the
199 enclosure when the flame exits the vent, which can be calculated for the example shown in
200 Fig. 1(b) as:

201 $$R_e=\left(\frac{3\cdot V}{4\pi}\right)^{\frac{1}{3}}=\left(\frac{3\cdot\frac{4}{3}\pi\frac{L}{2}\cdot R^2}{4\pi}\right)^{\frac{1}{3}}=\left(\frac{L}{2}(\sigma\cdot S_u\cdot t)^2\right)^{\frac{1}{3}} \tag{11}$$

202 In the equation (10), $S_u(t)A_f(t)$ is the effective flame surface area growth.

203 $$S_u(t)A_f(t)=4\pi\sigma\cdot S_u R^2\cdot\Xi(t) \tag{12}$$

204 where $\Xi(t)$ is the flame wrinkling factor, which is assumed to grow linearly with time, i.e.
205 $\Xi(t)=1+\Xi_o\cdot t$. Therefore, by combining the equations of (10) to (12), the maximum
206 external explosion pressure equation becomes:

207 $$\frac{P_e}{P_o}-1=\frac{\gamma(\sigma-1)\sigma\cdot S_u R_e\cdot\Xi_o}{a_0^2} \tag{13}$$

208 The calculation of the flame wrinkling factor Ξ_o is due to Taylor instability, which is
209 represented as $\Xi_o=(\Gamma_T a)^{1/2}$. Γ_T is a constant, which can be determined according to different
210 test results. a is the flame acceleration in the Rayleigh-Taylor unstable direction (Bauwens et
211 al., 2008):

212 $$a = \frac{2\sigma(\sigma-1)S_u^2 A_f}{A_v^{\frac{3}{2}}}\left[\sqrt{\frac{\sigma\cdot\gamma_p(\gamma_p-1)}{\gamma_r(\gamma_r-1)}}-1\right] \quad (14)$$

213 Therefore, the calculation of peak external pressure becomes:

214 $$\frac{P_e}{P_o}-1=\frac{\gamma(\sigma-1)\sigma\cdot S_u R_e}{a_0^2}\left\{\frac{\Gamma_T\, 2\sigma(\sigma-1)S_u^2 A_f}{A_v^{\frac{3}{2}}}\left[\sqrt{\frac{\sigma\cdot\gamma_p(\gamma_p-1)}{\gamma_r(\gamma_r-1)}}-1\right]\right\}^{1/2} \quad (15)$$

215 **2.2 Comparison of analytical results with experimental data (Enclosure fully filled**

216 **with 4.0 vol% propane-air mixture)**

217 The experimental data from (Bauwens et al., 2008; Bauwens et al., 2010) are utilized in the
218 comparison with the analytical results, as seen in Case No.1 to No.13 in Table 1. In the tests,
219 the gas concentration of propane-air mixture is 4.0 vol %, the vented gas is assumed to
220 consist of 10% unburned reactants and 90% of burned products. The ratios of specific heat
221 for product γ_p and γ_r are 1.26 and 1.4, respectively. The expansion coefficient σ, which is
222 the ratio of reactant density to product density, is 8.0 at temperature of 298K. The initial
223 burning velocity of the propane-air mixture S_u is estimated as the laminar value of propane of
224 0.4m/s. The dimensions of the test enclosure are 4.6 × 4.6 × 3.0 m. The testing vent areas are
225 2.7 m^2 and 5.4 m^2, respectively. The constant of Γ_T is chosen as 1.39×10^3 for the external
226 explosion pressure calculation near the vent opening. Back ignition and centre ignition
227 explosions are investigated in the comparison.

228 To determine the time *t*, when flame exits the vent opening, the flame time-of-arrival data
229 recorded in (Bauwens et al., 2011) are used. Precisely, the time is calculated according to the
230 recorded flame speed data and corresponding distance from ignition to flame location, as seen
231 in Fig. 2. However, the data of gas explosions are only provided for cases with centre ignition
232 at 2.73 m^2 vent (i.e. Case No. 2 & 3) and back-wall ignition at 5.43 m^2 vent (i.e. Case No. 4

& 5). In Fig. 2(a), the velocity at the vent exit for centre ignition with a 2.73 m^2 vent area is calculated as 44.55 m/s (U_o = 3.3 m/s), while the velocity is determined as 57.75 m/s for flame exits the vent from a back-wall ignition with a 5.43 m^2 vent area (in Fig. 2(b)). The flame velocity develops approximately in a linear growth rate, therefore, a factor of 0.8 is used to average the developing velocity from ignition to vent $v_{avr} = 0.8 * v$. The exit time *t*, is eventually determined as $t = 2D_{ignition-vent}/v_{avr}$. Namely, $t_{cen-2.73vent} = 2 \times \frac{2.3}{0.8\times44.55} = 0.129\ s$, $t_{back-5.43vent} = 2 \times \frac{4.6}{0.8\times57.75} = 0.199\ s$.

For Case No. 1 and 6-13, the flame developing times are estimated by conducting CFD simulation as reference. FLACS is used to simulate the back-wall and centre ignition explosions and to calibrate with experimental data, the detail of FLACS simulation will be introduced in Section 3. All CFD simulation setups are kept constant expect the varying ignition locations and obstacle arrangements. As seen in Fig. 3, from the back-wall ignition (top figure in Fig. 3(a)) to centre ignition (top figure in Fig. 3(b)), the comparison indicates the flame exiting vent time decreases from 0.199s to 0.150s. Therefore, 0.150s is used to Case No. 6 & 7, and a decreasing factor of 0.75 is seen. $t_{back-2.73vent} = \frac{0.129}{0.75} = 0.172\ s$ is used for Case No. 1. Furthermore, the top figure and bottom figure in Fig. 3(b) show that the flame exists the vent nearly at the same time (0.150s) for centre ignition scenarios with and without obstacles. Hence, 0.150 s is also used for Case No. 11-13, and 0.129 s is used to Case No. 8-9 with obstacles that are consistent with Case No. 2-3 without obstacles. Lastly, bottom figure in Fig. 3(a) indicates the flame exiting time of 0.180s for case No. 10.

In addition to the experiments of (Bauwens et al., 2010), other vented gas explosion data are also compared with the modelled results. For example, the 12.5 vol % methane-air mixture tests in a 2 × 2 × 3.0 m enclosure by (Li et al., 2017b; Li et al., 2017c), the 18 vol % hydrogen explosion in an enclosure with dimension of 1 × 1 × 1 m conducted by (Kuznetsov

et al., 2015) and 30 vol % vented hydrogen explosion testing in an small-scale enclosure (i.e. 0.15 × 0.15 × 0.15 m) by (Rocourt et al., 2014) are included in the analytical model validation. The time data when flame exits the vent opening recorded from the above tests are also summarized in Table 1 and utilized to calculate the sphere radius R_e in the equation (10).

By applying all parameter values into the equation (15), all internal peak pressures due to external explosion near the vent are calculated and indicated in Fig. 4.

Table 1 Comparison of analytical results with test recorded data

Case No.	Ignition location	Vent size (m2)	Enclosure dimension (m)	Gas concentration	BR *	Time flame exit vent (s)	Measured P1 (bar)	Modelled P1(bar)
1	back	2.73	4.6x4.6x3	4% propane	0	0.172	0.132	0.115
2	centre	2.73	4.6x4.6x3	4% propane	0	0.129	0.035	0.023
3	centre	2.73	4.6x4.6x3	4% propane	0	0.129	0.041	0.023
4	back	5.43	4.6x4.6x3	4% propane	0	0.199	0.056	0.076
5	back	5.43	4.6x4.6x3	4% propane	0	0.199	0.060	0.076
6	centre	5.43	4.6x4.6x3	4% propane	0	0.150	0.025	0.017
7	centre	5.43	4.6x4.6x3	4% propane	0	0.150	0.016	0.017
8	centre	2.73	4.6x4.6x3	4% propane	6%	0.129	0.048	0.039
9	centre	2.73	4.6x4.6x3	4% propane	6%	0.129	0.06	0.039
10	back	5.43	4.6x4.6x3	4% propane	6%	0.180	0.186	0.174
11	centre	5.43	4.6x4.6x3	4% propane	6%	0.150	0.027	0.030
12	centre	5.43	4.6x4.6x3	4% propane	6%	0.150	0.025	0.030
13	centre	5.43	4.6x4.6x3	4% propane	6%	0.150	0.031	0.030
14[#]	back	0.5	1x1x1	18% hydrogen	0	0.085	0.125	0.110
15[#]	back	0.008	0.15^3	30% hydrogen	0	0.004	0.250	0.220
16[#]	centre	0.008	0.15^3	30% hydrogen	0	0.004	0.110	0.078
17[#]	centre	0.064	2x2x3	12.5%methane	0	0.180	0.020	0.039

[*] *BR* represents the blockage ratio. The effect of obstacle on peak pressure calculation is increasing the flame area, which is expressed as: $A_f^{obstacle} = A_f\,[1+1.333\sigma^{0.14}(2BR)^{0.86}]^2$ for far-end ignition, $A_f^{obstacle} = A_f\,[1+1.333\sigma^{0.14}(0.5BR)^{0.86}]^2$ for centre ignition (Bauwens et al., 2010). [#] Case No.14 data are from Kuznetsov et al., 2015, Case No.15 & 16 data are from Rocourt et al., 2014, Case No.17 data are from Li et al., 2017b, and other case results are extracted from Bauwens et al., 2010.

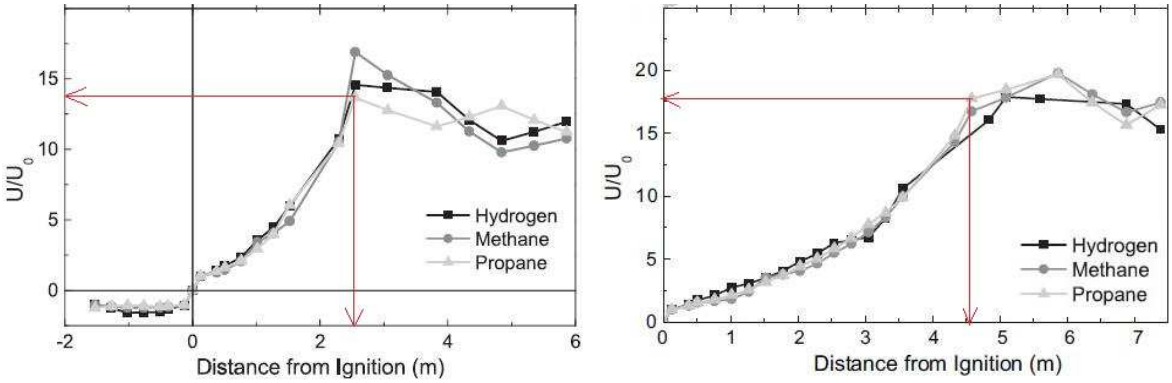

271

272 **(a) Initial flame speed for hydrogen, methane and**
273 **propane gases for centre ignition with a 2.7m^2 vent**

(b) Initial flame speed for hydrogen, methane propane for back ignition with a 5.4m^2 vent

274 **Fig. 2 Initial flame speed for hydrogen, methane and propane mixtures with different**
275 **ignition and vent area conditions, U_o=3.31m/s (Bauwens et al., 2011)**

276

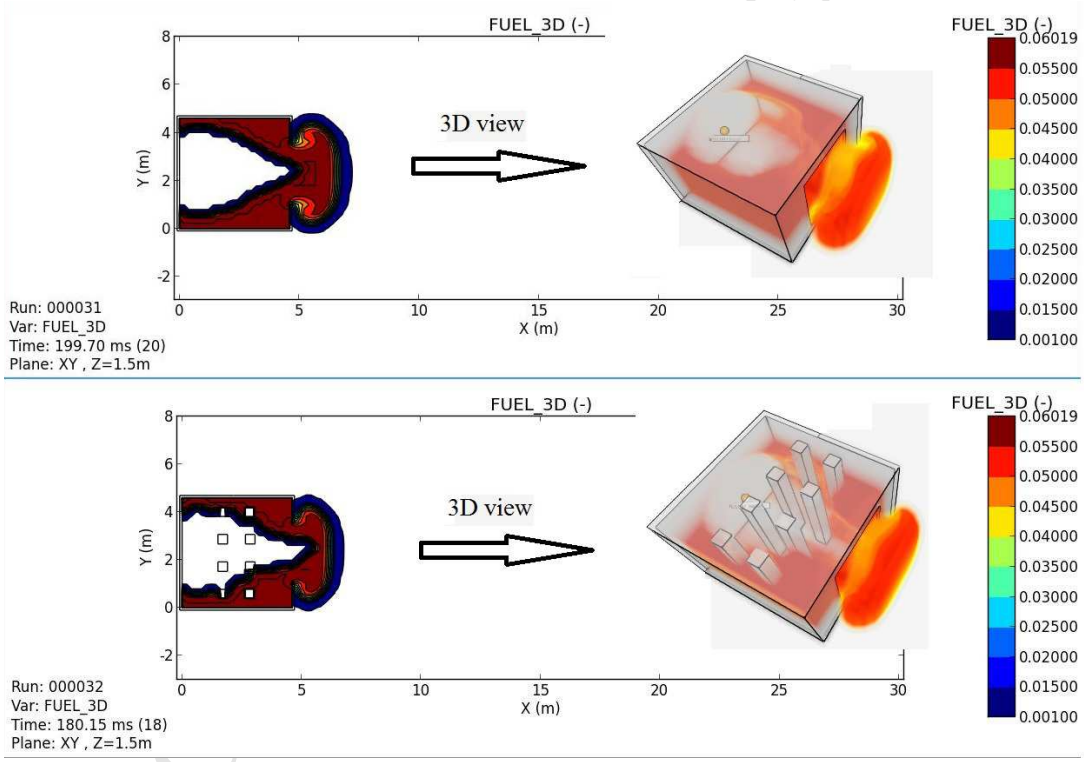

277
278 **(a) Back-wall ignition scenarios with and without obstacles**

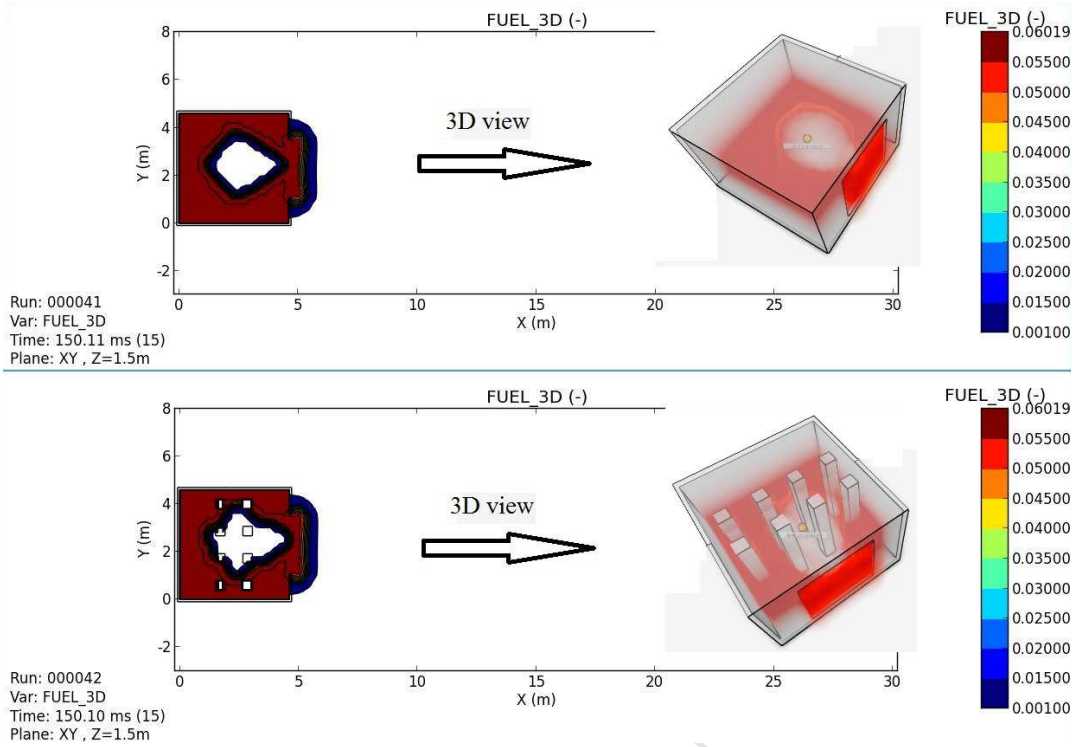

(b) Centre ignition scenarios with and without obstacles

Fig. 3 Gas cloud transformation during explosion

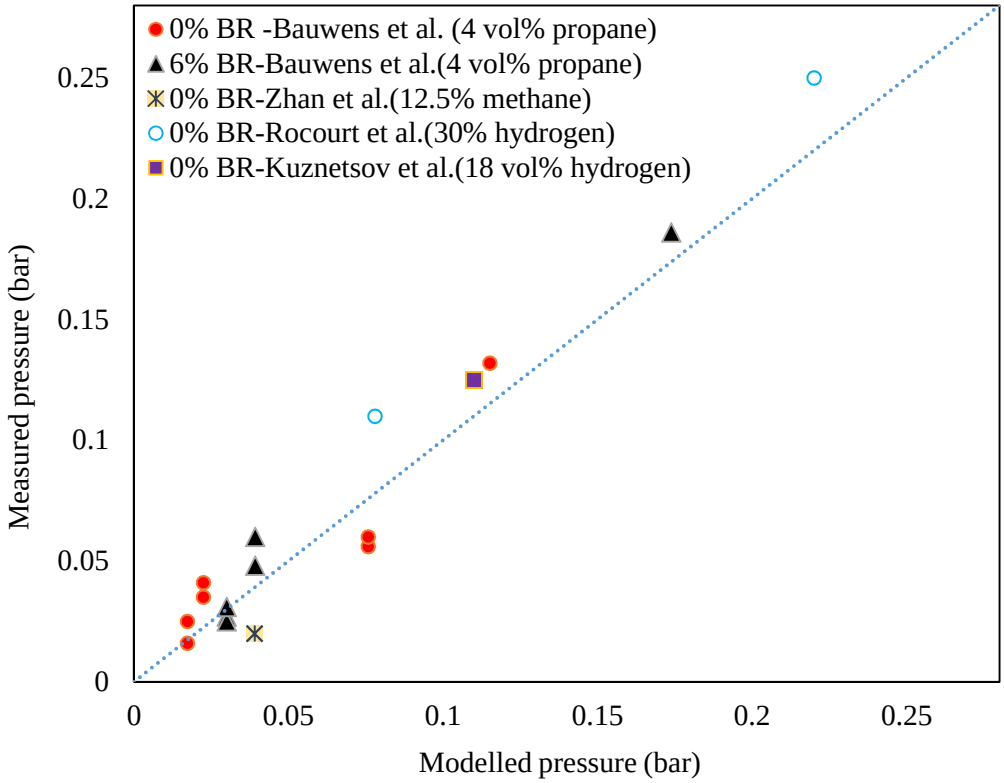

Fig. 4 Comparison of test results and analytical data for peak pressures near the vent due to external explosion

As shown in Fig. 4, satisfactory agreement is seen between the experimental data and analytically calculated results for vented gas explosions with different vent sizes, ignition locations and existence of obstacles. However, the parameter of Γ_T is determined by trial and error method. For different experiments in different scales, different values of Γ_T should be used to achieve a good prediction. Moreover, the time t when flame exists the vent is determined according to the experimental reading. In other words, some parameters need be determined with experimental data for the analytical approach to achieve good predictions. For an unexpected explosion in reality, the critical time when the venting initiates and when the flame nose tip reaches the vent opening cannot be straightforwardly predicted without using recorded data. Therefore, how to use the above analytical model to estimate the explosion pressure without knowing the critical venting time becomes a conundrum.

2.3 Comparison of analytical results with experimental data (Enclosure filled with 10 vol% layered methane-air mixture)

In the comparison above, the flammable gas-air mixture is ideally mixed in all tests and the correlations are developed based on the well-mixed explosions. In reality, accidental gas leakage within chambers and buildings are likely to generate flammable mixtures with inefficient mixing. Therefore, gas concentration layering is expected to occur. Especially when the gas mixture is lighter than air, a certain amount of such gas leakage eventually will lead to layered flammable vapor cloud on the top of the enclosure.

For example, in the experiments performed by (Palmer and Tonkin, 1980), 10 vol % methane-air mixture with several different layer depths were seen in the large room with dimensions of 3.9 × 3 × 2.4 m. Same as the comparison above, the analytical models are used to predict the experimental results with layered methane-air mixture to further check their accuracy and applicability.

The combustion is assumed under adiabatic process, the thermodynamic parameters of unburned and burned 10 vol % methane-air mixture, which are obtained according to (Gordon and McBride, 1994; Ferguson and Kirkpatrick, 2015), are summarized in Table 2. A set of different methane-air mixture layer depths are listed in

Table 3 . The vent area is $0.9m^2$ (i.e. 1/8 vent ratio of the front wall).

Table 2 Thermodynamic parameters of unburned and burned methane-air mixture of 10 % volume concentration

	M **(kg/kmol)**	γ	***T*** **(K)**	σ	**P**
Reactants	27.64	1.39	298.15	7.6	1 ATM
Products	27.16	1.21	2225.5	-	-

The peak internal pressures in

Table 3 are calculated by substituting all parameters in Table 2 into the equations (8) to (15). It is seen that the analytically estimated pressures are higher than recorded data, especially for smaller layer depth cases. The main reason is that the flame area calculation in the equation (8) is based on the explosion occurring in fully filled enclosure with stoichiometric gas-air mixture, as seen in Fig. 1(a) and Fig. 5(a). However, for enclosures with layered gas-air mixture, such as the case in Fig. 5(b), the flame expansion is not confined in all boundaries. After ignition on the interface between the fuel mixture and air, the gas-air mixture will expand into the bottom with a remixing procedure to some degree. Therefore, the combustion should have a smaller flame area in flame propagation direction towards the vent opening. A flame area adjusting parameter is defined to calculate the flame area of layered gas-air mixture in the enclosure:

$$\Psi = \left(\frac{D_l}{3 \cdot D_v} \right)^{1.2} \tag{16}$$

$$A_{f,\mathrm{mod}} = \Psi A_f \tag{17}$$

where D_l is the layer depth of the gas-air mixture, D_v is the vent opening depth, $A_{f,mod}$ is the modified flame area in the enclosure with layered mixture.

Table 3 Layer depths, recorded peak internal pressures in tests and estimated peak pressures by analytical models

Layer depth[#] (m)	$P_{i,exp}$[#] (kPa)	$P_{i,ana}$^ (kPa)	A_f (m^2)	$A_{f,mod}$^ (m^2)
0.50	4.30	10.21	19.29	4.15
0.60	5.60	10.28	19.55	5.23
0.90	6.19	10.53	20.48	8.92
1.20	7.75	10.81	21.59	13.27
1.50	9.29	11.12	22.84	18.35
1.80	11.75	11.44	24.20	24.20

^ $A_{f,mod}$ is the modified flame area, $P_{i,ana}$ is the calculated peak internal pressure by analytical models. [#] the data of layer depths and maximum internal pressure are extracted from (Palmer and Tonkin, 1980).

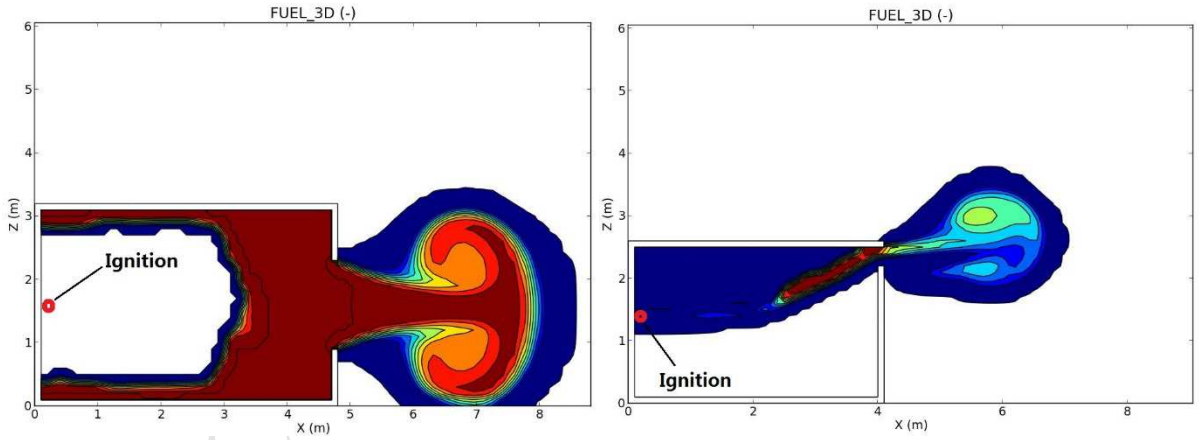

(a) Enclosure fully filled with gas mixture **(b) Enclosure with layered gas mixture**

Fig. 5 CFD modelled flame areas for demonstration purpose

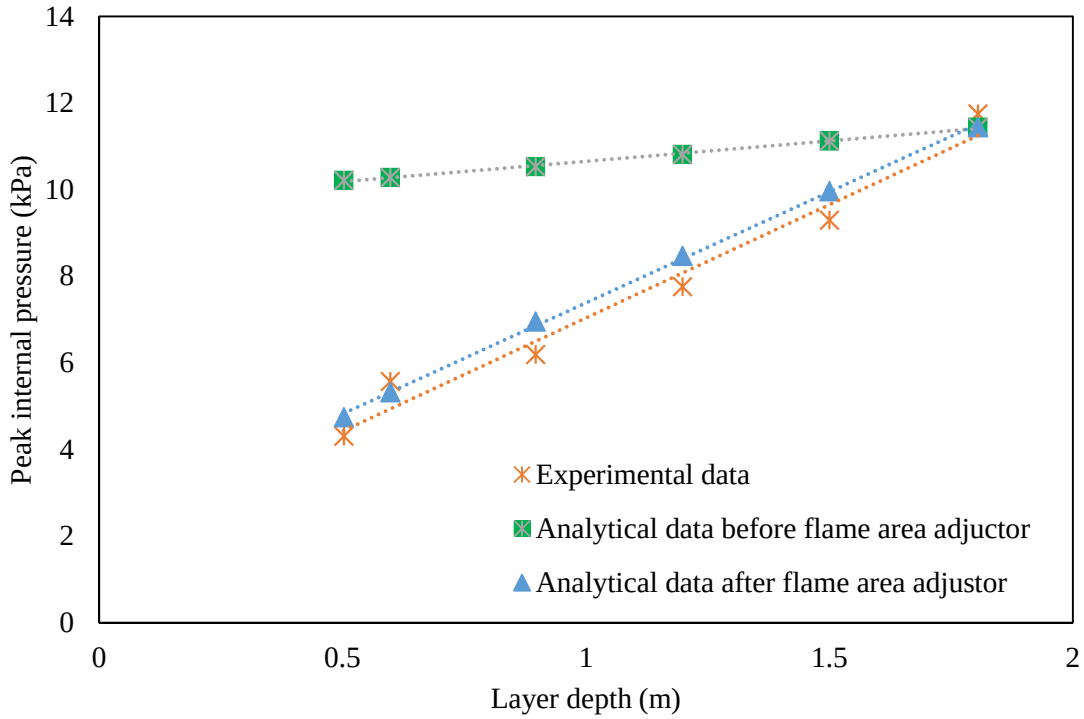

Fig. 6 Peak internal pressures with different layer depths of gas mixture

By using the factor of Ψ, the peak internal pressures inside the 3.9 × 3 × 2.4 m enclosure are recalculated and shown in Fig. 6. It is observed that the analytically estimated peak pressures agree well with experimental results. However, the comparison above is only based on 6 sets of experimental data. The determinations of the factors of Γ_T and flame venting initiation time *t* are still inconclusive. Moreover, the assumptions above are idealized, and these models are only capable of predicting the internal peak pressures near the vent but not the subsequent external pressures. For a more realistic vented explosion with more uncertainties, for the cases without the corresponding testing data to determine the respective parameters for the analytical models, and for the situations that need to determine the blast wave propagation outside the enclosures for estimation of external pressures, CFD simulation is suggested.

3 CFD simulation and validation

3.1 Vented explosion simulation by using FLACS

The CFD-based software FLACS of version 10.4 (Gexcon, 2015) , which relies on turbulence models based on Reynolds-averaged Navier-Stokes (RANS) equations (i.e. k–ε model for turbulence simulation), is firstly employed to simulate the vented gas explosion. In order to ensure good representation of flame area inside the vented explosion, the Simple Interface Flame (SIF) model (Arntzen, 1998) is applied to calculate the compressible flows.

In the preprocessor CASD of FLACS, the 3.9 × 3 × 2.4 m explosion enclosures with varying vent areas are as shown in Fig. 7. All walls of the enclosure are modelled as rigid in the CFD simulation since the roof and walls in the experiments were made of steel plates and the floor was of concrete. The depths of the vent are 0.3m, 0.9m and 1.2m, giving vent ratios of the front wall between 12.5% and 50%. The lightweight polyethylene sheet of 0.05mm thick is modelled as POPOUT relief panel in FLACS. Vent opening pressure is set at 0.7 kPa. The ignition starts at the interface between the underlying air and fuel-air mixture layer, and it is located centrally within the large enclosure near the back wall remote from the vent area as seen in Fig. 8.

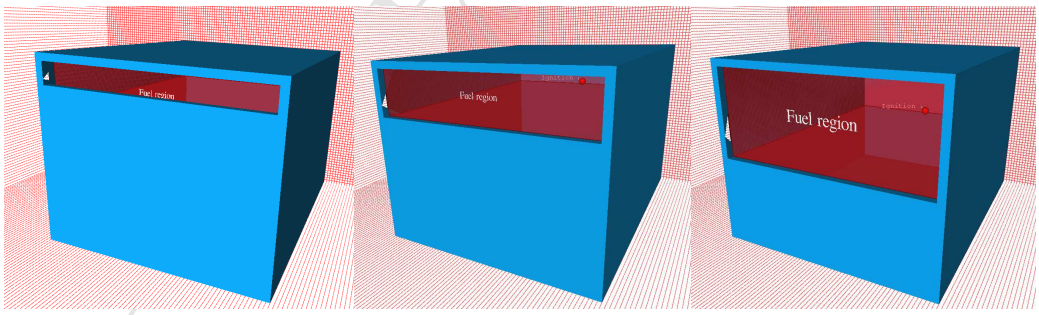

Fig. 7 3D models of explosion enclosure with different vent areas

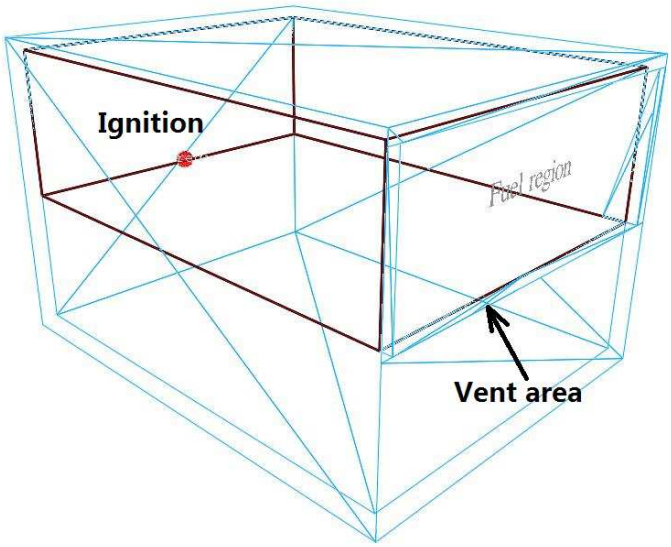

Fig. 8 Fuel-air mixture layer depth, ignition and vent area location

Euler boundary condition is applied, room temperature of 26 degree and atmosphere pressure 101 kPa are used as initial conditions. The fuel-air mixture's volume concentration is 10%. Grid cells are cubical inside the enclosure to reduce the deviations of flame propagation and overpressure built-up, whereas grid cells are stretched from vent panel to outside boundaries in the air. The aspect ratio of the grid increment was controlled within 10%. The grid size within the enclosure is decided as 0.05m based on the grid cell sensitivity study. Monitor points are allocated near the wall and the vent to record the peak internal pressures.

In the literature of (Palmer and Tonkin, 1980), only the maximum pressures were recorded, which are used in the present study to verify the accuracy of the numerical simulations. The layer depths, internal pressures near the vent and external pressure at 9.1m and 18.3m from experiments are extracted and tabulated in Table 4. The experimental case with 0.6m fuel-air mixture layer and 12.5% of vent area is numerically modelled by using FLACS. Fig. 9(a) shows the recorded pressures near the vent and in the far field, while the corresponding 3D view of fuel mass fraction of the flame during the vented explosion (i.e. the case No. 4 in Table 4) is shown in Fig. 9(b). It is seen that the procedure of fuel-air mixture consumption and the propagation of the mixture cloud are well modelled by using FLACS.

In terms of the CFD simulated pressure, the pressure-time history data near the vent of case No. 4 are extracted from FLACS postprocessor of Flowvis and shown in Fig. 10. The venting of burned products from the enclosure is seen at time of 0.14s with an opening pressure of approximately 0.8kPa in Fig. 16, and the maximum pressure is monitored at 5.8kPa, which is close to the experimental data. In order to thoroughly validate the FLACS estimated results, all peak pressures extracted from simulation cases in Table 4 are compared with experimental data, as seen in Fig. 11. A good agreement between the maximum internal pressure estimated by FLACS and that recorded in experiments is observed. Furthermore, it is seen that the maximum pressures increase unanimously with the ratio increment of fuel mixture layer depth to vent opening depth for all simulation cases.

Table 4 Recorded maximum internal pressures, external pressures, fuel layer depths and vent areas (Palmer and Tonkin, 1980)

Case No.	Internal peak pressure (kPa)	Gas-air mixture layer depth (m)	Vent area (m^2)	External pressure at 9m (kPa)	External pressure at 18.3m (kPa)
1	1.32	1.25	3.60	0.44	0.19
2	1.94	0.72	1.80	0.50	0.22
3	4.27	0.50	0.90	0.66	0.31
4	5.58	0.60	0.90	0.78	0.48
5	6.68	1.80	1.80	1.40	0.71
6	9.33	1.50	0.90	3.19	1.53
7	11.66	1.80	0.90	3.37	2.00

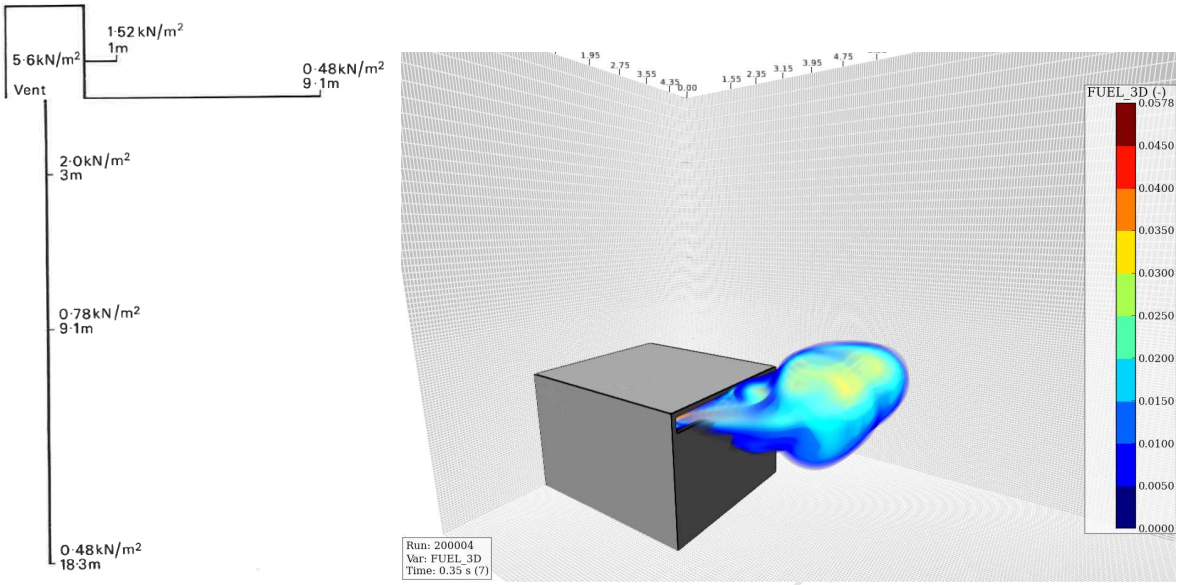

(a) Recorded peak pressures for test with 12.5% vent area (Palmer and Tonkin, 1980) and corresponding case No. 4 in Table 4

(b) 3D view of fuel mass fraction during combustion of case No. 4

Fig. 9 Recorded pressures in experiment and numerical modelling 3D view of Case No. 4

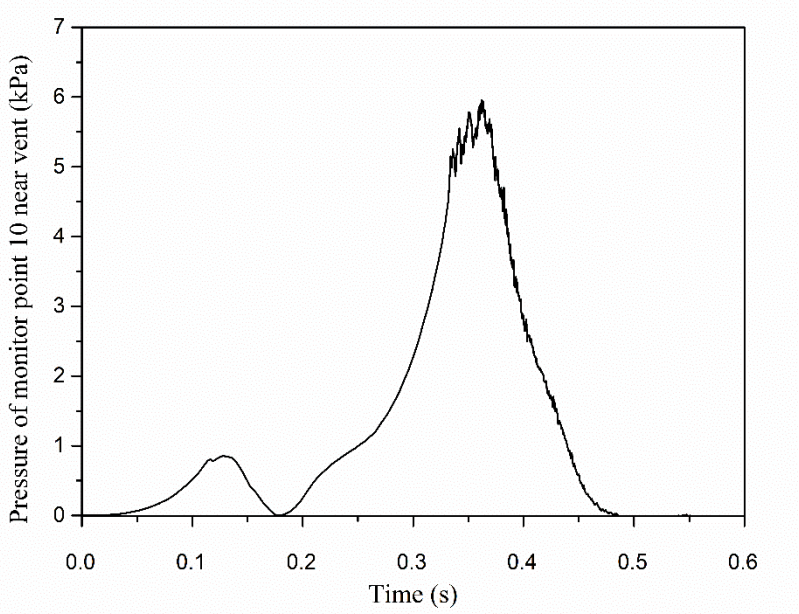

Fig. 10 Pressures monitored near the vent of case No. 4 in FLACS simulation

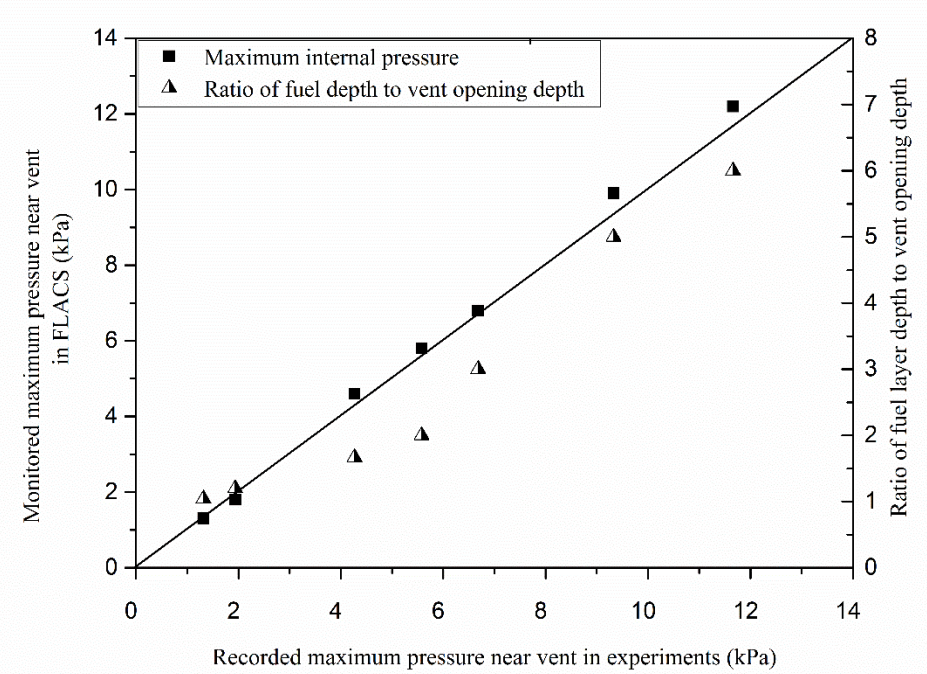

412
413 **Fig. 11 Comparison of FLACS modelled pressures to experimental data recorded near vent**
414

415

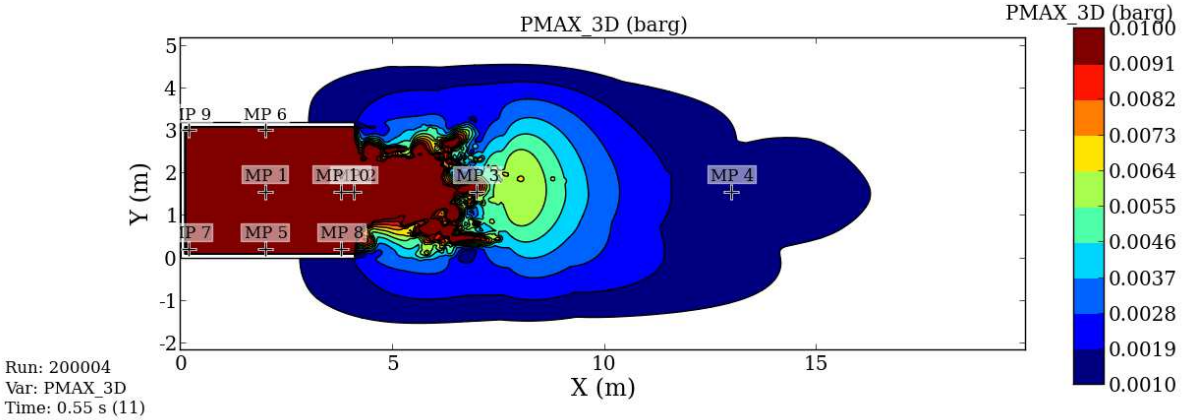

416

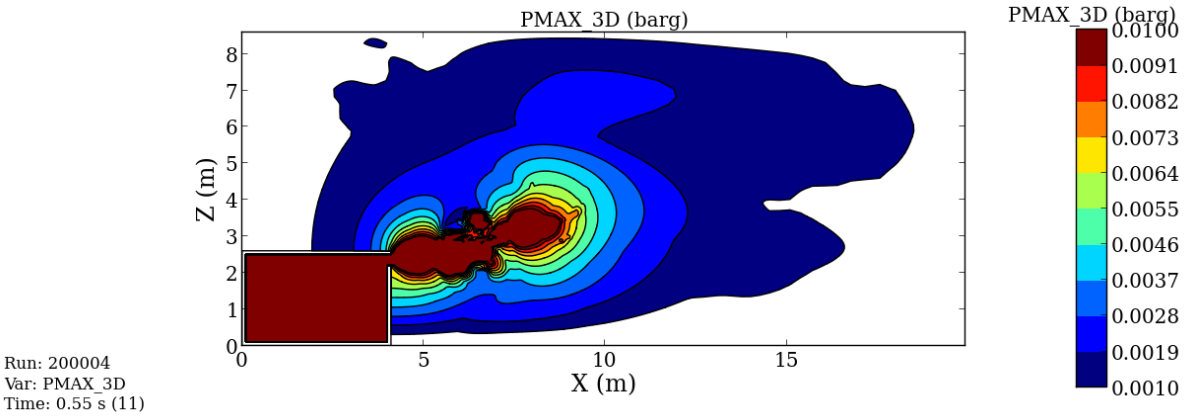

417

418 **Fig. 12 Plan view (top figure) and side view (bottom figure) of the maximum pressure in case No.**
419 **4 after the FLACS far-field pressure guideline by (Hansen and Johnson, 2015)**

The new pressure prediction guideline (Hansen and Johnson, 2015) is applied in the far-field blast propagation simulation of FLACS. The sound velocity and flame fluid velocity based CFLV and CFLV numbers are both reduced to 0.1 by using cn-files, the numerical time step is therefore decreased to prevent excessive numerical smearing of blast waves. However, due to the fact that the external blast waves in this study are from low pressure deflagration, the DPDX factors are much smaller than 0.5, which is the threshold of DDT in the new guideline. Consequently, the date-dump (Ma et al., 2014) is decided to start at the time the burned products exit the vent opening. A new dump-file is then restarted with a non-reflecting boundary condition of "PLANE_WAVE".

Comparing to the recorded pressures, namely 2kPa and 0.78kPa at the distances of 3m and 9.1m away the vent area in Fig. 9(a), the far-field pressures (i.e. 0.9kPa and 0.1kPa) in Fig. 12 are significantly under-estimated by using FLACS. It is concluded that without the correct indication of DPDX parameter, which is commonly used in highly congested gas explosion simulation, the new far-field blast prediction guideline of FLACS cannot be well utilized for the vented explosion with slow deflagration. In order to well simulate the low turbulent flame propagation in far field, the ANSYS Fluent is utilized in the following section.

3.2 External pressure prediction by using ANSYS Fluent

In accordance with the $k-\varepsilon$ model used in FLACS, the Navier-Stokes (RANS) equations are also chosen for turbulent flow simulation in ANSYS Fluent. In the above comparison of FLACS simulations with experimental results, the estimated internal pressures near the vent by using FLACS are proved to be accurate. Therefore, the pressure-time curves (e.g. data in Fig. 16) extracted from FLACS simulations are used as the input in ANSYS Fluent to model the subsequent flame propagation. In other words, the numerical chemical reaction of

combustion and the stoichiometric reactions are performed in FLACS simulation, but the vented products and wave propagation after combustion are calculated in ANSYS Fluent.

The geometry of the vented gas explosion with layered fuel mixture in ANSYS Fluent is modeled according to the experimental setup (Palmer and Tonkin, 1980), where the back wall and the bottom of the vented enclosure room are modelled as a concrete wall and ground. The 3D modelled enclosure as shown in Fig. 13 has the same dimensions of 3.9 × 3 × 2.4 m in the test. The ANSYS CFD preprocessor - ICEM (Ansys, 2015), which provided mesh generation and advanced geometry acquisition, is employed. The hexahedral cell sizes of 0.05m, 0.1m and 0.15m stretching from the vent opening are tested in the sensitivity study. The 0.1m cell for the vent area is decided so that about 100 cells and 200 cells for 12.5% and 25% vent ratio openings, respectively, are used.

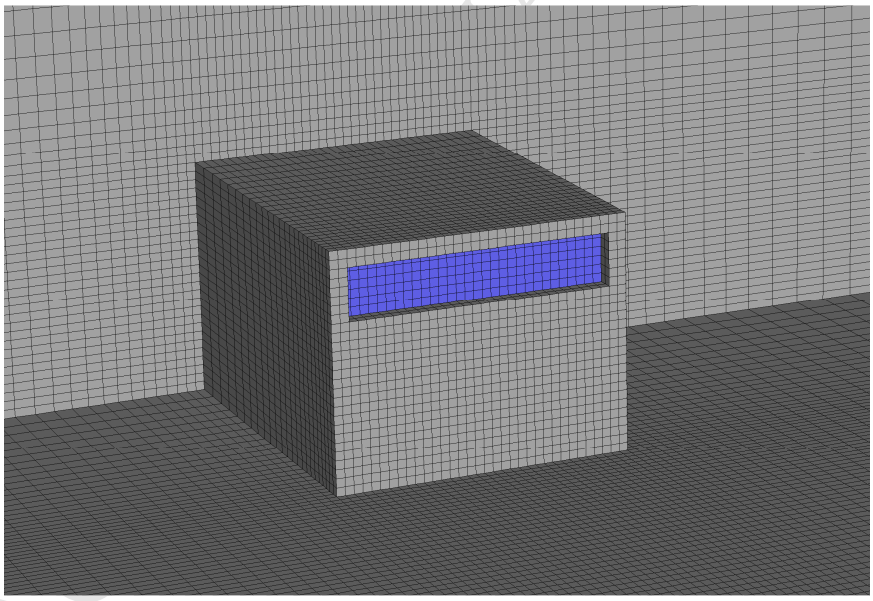

Fig. 13 3D geometry of the vented enclosure with 25% vent area on front wall in ANSYS Fluent

Symmetry boundary is used for half size of the enclosure modelling, which enables acceleration of computational calculation time. The overall boundary and meshing are shown in Fig. 14 with dimensions of 50 × 30 × 15m, the enclosure with dimensions of 3.9 × 3 × 2.4 m is placed in the middle and near the boundary on the left hand side. The meth stretching factor is about 1.01 from the vent area in x, y and z directions. In total, there are 1×10^6

hexahedral cells, and 3×10^6 quadrilateral interior faces for the entire domain. The mesh quality is controlled with the maximum Ortho Skew of 9.6×10^{-10}.

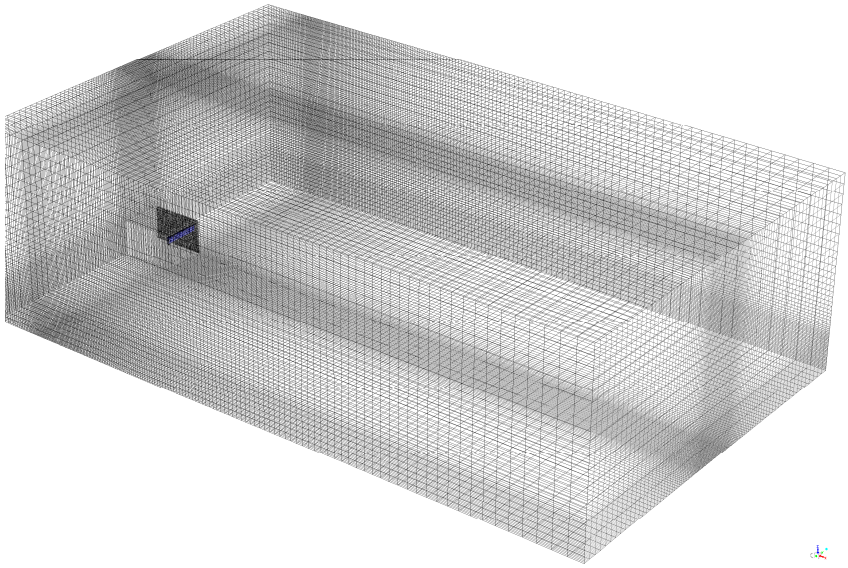

Fig. 14 CFD simulation boundary and mesh generation for the vented enclosure in ANSYS Fluent

The density-based solver and transient solution are used to solve the governing equations of continuity, momentum and energy etc in the coupled-implicit formulation. The gravitational acceleration is in *z*-direction. Standard k-ε model and standard wall functions are applied in the modelling along with the energy equation model. Ideal gas material is chosen to simulate the air outside the enclosure, while concrete and steel materials are selected for the concrete ground and enclosure walls, respectively. The initial operating pressure is set as zero pascal, and overpressures above the ambient air pressure are imported to the pressure-inlet boundary. Operating temperature is 288K.

The enclosure's walls are modelled as stationary without slip, the thermal condition is assumed as adiabatic with zero heat flux, wall thickness is 0.01m. The concrete wall and ground are also modelled as adiabatic with thickness of 0.1m. Low back flow turbulent intensity and viscosity ratio (i.e. 1%) are used, and the backflow total temperature is kept constant at 288K with acoustic wave model turned off for the initial pressure outlet boundary.

The pressure inlet boundary is set at the vent opening, where zero initial gauge pressure is used.

An UDF(Fluent, 2012) file is created to import the pressure-time history data. The simplified pressure-time data, as seen in Fig. 16, is compiled as the UDF file. The determination of such simplified pressure-time data as pressure inlet input is based on the assumptions below:

For a pressure inlet boundary in ANSYS Fluent, it is known that the total pressure should be determined as the input, namely

$$P_{Total\,pressure} = P_{gauge/static\,pressure} + P_{dynamic\,pressure} \tag{18}$$

$$P_{dynamic\ \ pressure} = \frac{1}{2}\rho v^2 \tag{19}$$

$P_{gauge/static\ \ pressure}$ is shown in top figure of Fig. 15 (corresponding to the pressure output in Fig. 10), while $P_{dynamic\ \ pressure}$ in Equation 18 and 19 is attributed to the kinetic energy at the vent. To calculate the dynamic pressure $P_{dynamic\ \ pressure}$, the flame velocity data extracted from FLACS (as shown in bottom figure of Fig. 15) is used. It is seen that the peak flame velocity at the vent exit is about 50 m/s. Therefore, for methane with density ρ of 0.668 kg/m^3, the peak dynamic pressure due to kinetic energy is equal to 0.835 kPa (i.e. $P_{dynamic\ \ pressure} = 0.5 \cdot 0.668 \cdot 50^2$ =0.835 kPa). Overall, the dynamic pressure contributes to about 12.6% in total peak pressure of 6.635 kPa (i.e. $P_{Total\ pressure}$ = $P_{gauge/static\ \ pressure} + P_{dynamic\ \ pressure}$ = 5.8 kPa +0.835 kPa).

By integrating all flame velocity converted dynamic pressures into total pressures, the time history data are summarized and shown in Fig. 16. It is seen that the total pressures (green dash line in Fig. 16) are slightly higher than initial pressures from FLACS output (i.e.

pressure-time data in Fig. 10 or black solid line in Fig. 16). Moreover, in this study, the pressures of interest are in far field (i.e. 9m and 18m). The kinetic energy with peak flame velocity of 50 m/s at vent are much less influential in the far field compared to the blast wave propagating with a velocity over sound speed of 343m/s. Therefore, to predict the far-field pressures, the pressure inlet input data are simplified by neglecting the small kinetic energy near vent.

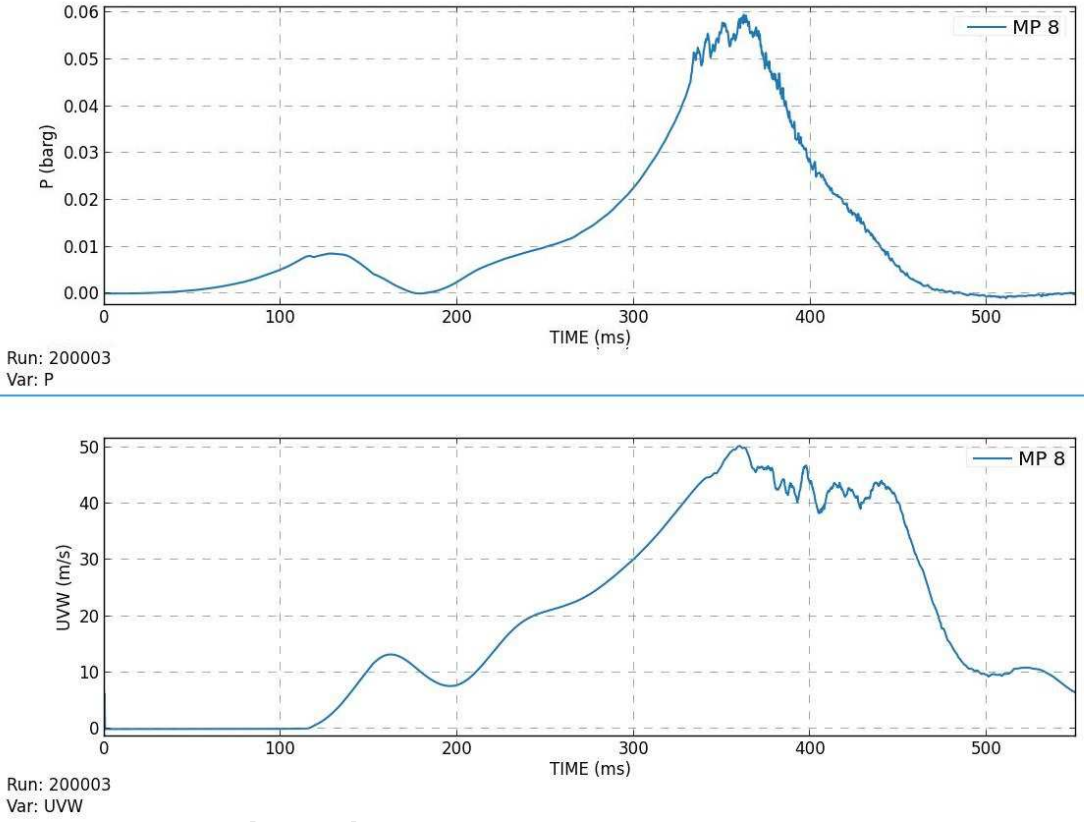

Fig. 15 Pressures-time history (top figure) and flame velocity-time history (bottom figure) monitored near the vent of case No. 4 in FLACS simulation

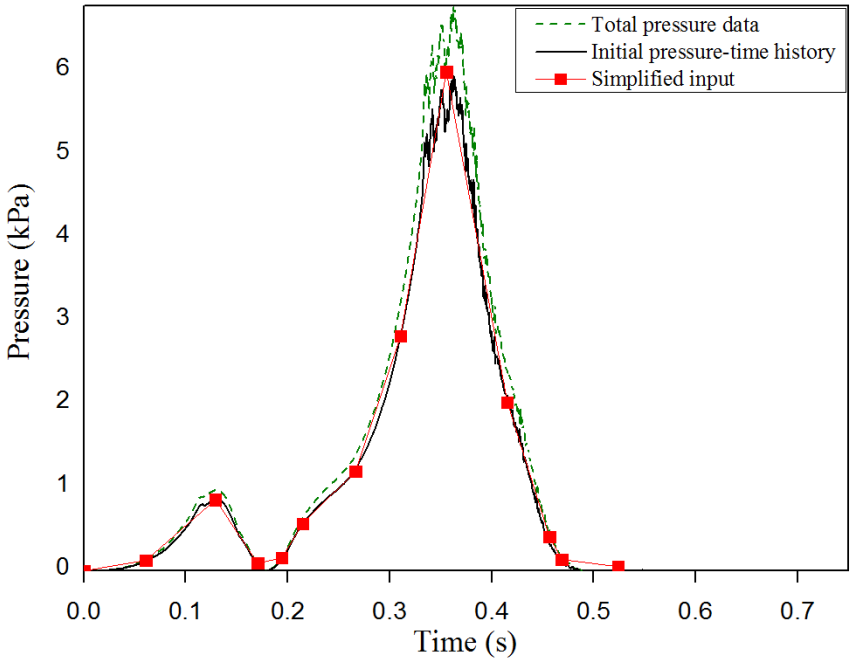

Fig. 16 Pressures monitored near the vent of case No. 4 in FLACS simulation, total pressure data and simplified pressure-time input

The pressure propagates normal to the boundary with intensity and hydraulic diameter calculation method for the turbulence modelling. Since the vent area has a rectangular shape, the hydraulic diameter is calculated as:

$$d_h = 4\frac{ab}{2(a+b)} \tag{20}$$

where a is the width and b is the height of the vent area.

The Advection Upstream Splitting Method (AUSM), which provides exact resolution of contact and shock discontinuities, is used for the convective flux calculation. Least squares cell based gradient is applied for the spatial discretization. Default relaxation factors are used with 10 courant number in the solution control.

One of the vented explosions in Table 4 - case No. 4 is chosen in following demonstration. The pressure-time history data from Fig. 16 are imported as the pressure inlet input. The simulation starts with a fixed time step size of 1×10^{-4} and finishes at time when external

pressure in far field decreases to zero. Convergence for each time set is guaranteed. In the CFD post software, the 3D results of external pressure at time of 0.355s (peak pressure time) are shown in Fig. 17. Due to the fact that the flame propagates perpendicularly to the vent area, which is modelled as a flat plan in ANSYS Fluent, the pressure distribution in 3D is shown in bullet shape with a diminishing trend.

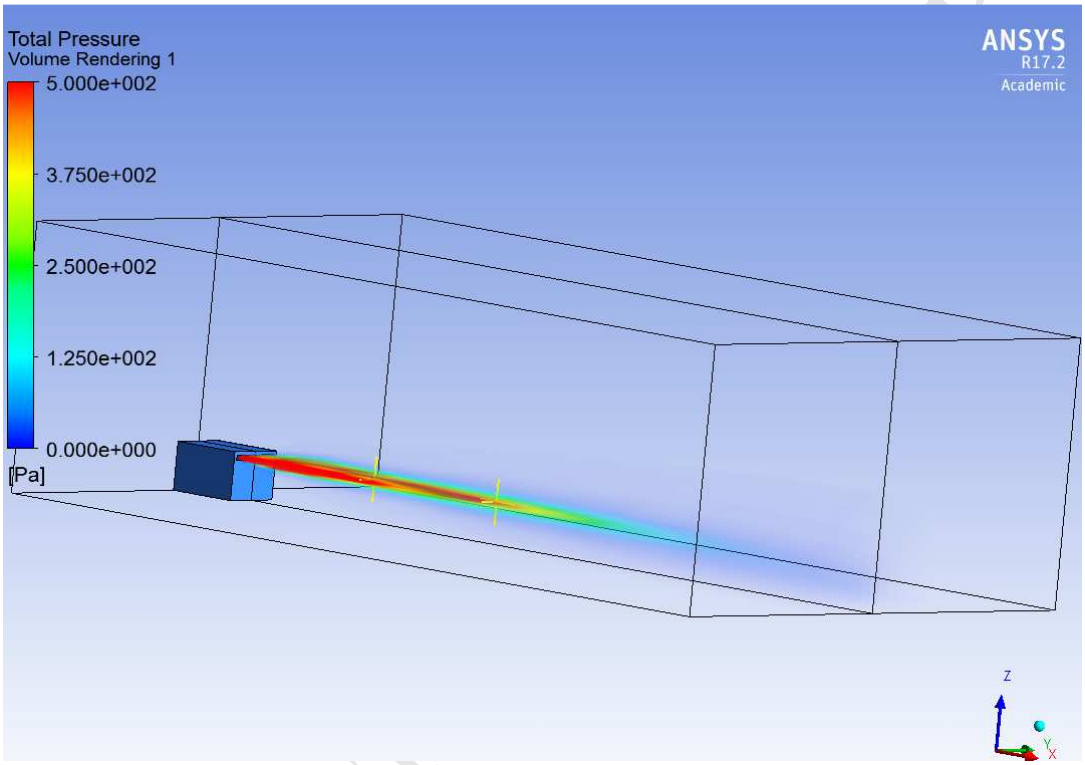

Fig. 17 Total pressure in the free air from the vented explosion in 3D model of ANSYS Fluent

The external pressure monitoring points are placed at 9.1m and 18.3m perpendicular to the vent area, as in the experimental test. The pressure-time history curves at these two points are shown in Fig. 18. As seen in the figure, the calculated pressure time-history with FLACS at the venting location is simplified as a series of linear curves in red color and used as input to ANSYS Fluent in the simulation. For the simulated external pressures at 9.1m and 18.3m, the output is recorded at every 40 time steps (time step size is 0.0001s) and also shown in the figure. The pressure-time history curves indicate that the peak pressure at 9.1m occurs about

543 0.02s after the peak pressure at the vent opening, while another 0.02s delay is seen for the
544 pressure wave to reach the peak at 18.3m.

545 The peak pressures at 9.1m and 18.3m in the CFD-post are recorded as 0.82kPa and 0.44kPa,
546 respectively. By comparing the CFD results with the experimental data in Fig. 9 (a), the
547 differences between the calculated and recorded peak pressures are 4.88% and 8.33% at the
548 two points, respectively. For all other vented explosion cases, the comparison of peak
549 pressures is shown in Fig. 19. Overall, the ANSYS Fluent calculated peak pressures in the
550 free air are close to the experimentally recorded maximum pressures.

551

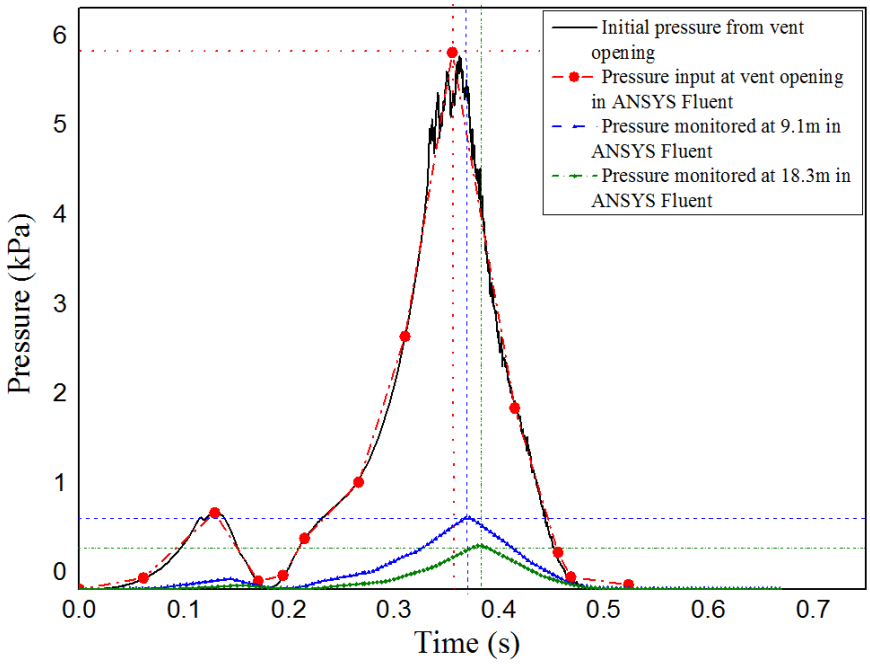

552

553 **Fig. 18 Data of pressure-time input near vent opening and external pressure-time output**
554 **monitored at 9.1m and 18.3m**

555

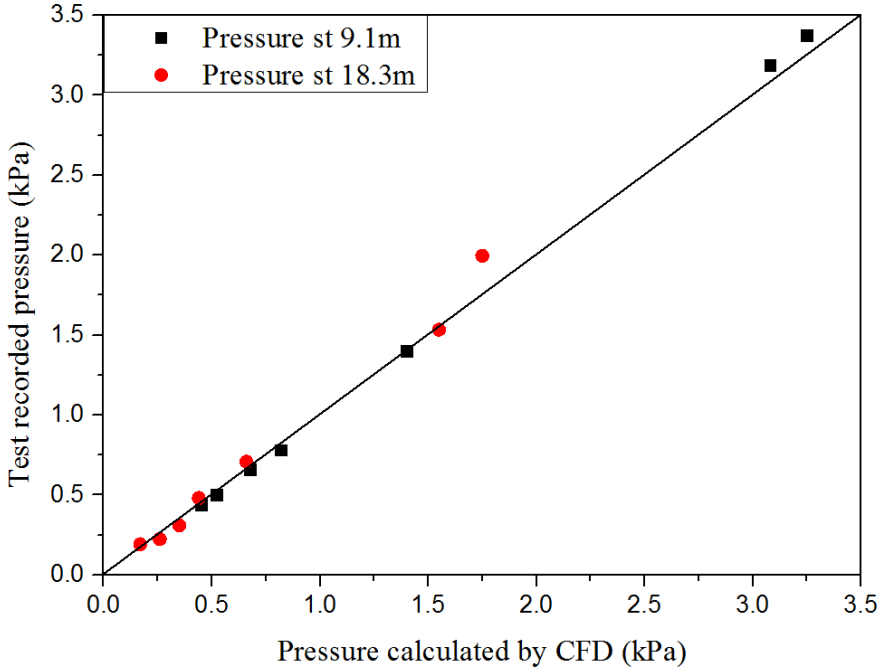

556

557 **Fig. 19 Comparison of the recorded and calculated maximum pressures at 9.1m and 18.3m**
558 **from the vent opening for all the tested cases in (Palmer and Tonkin, 1980)**

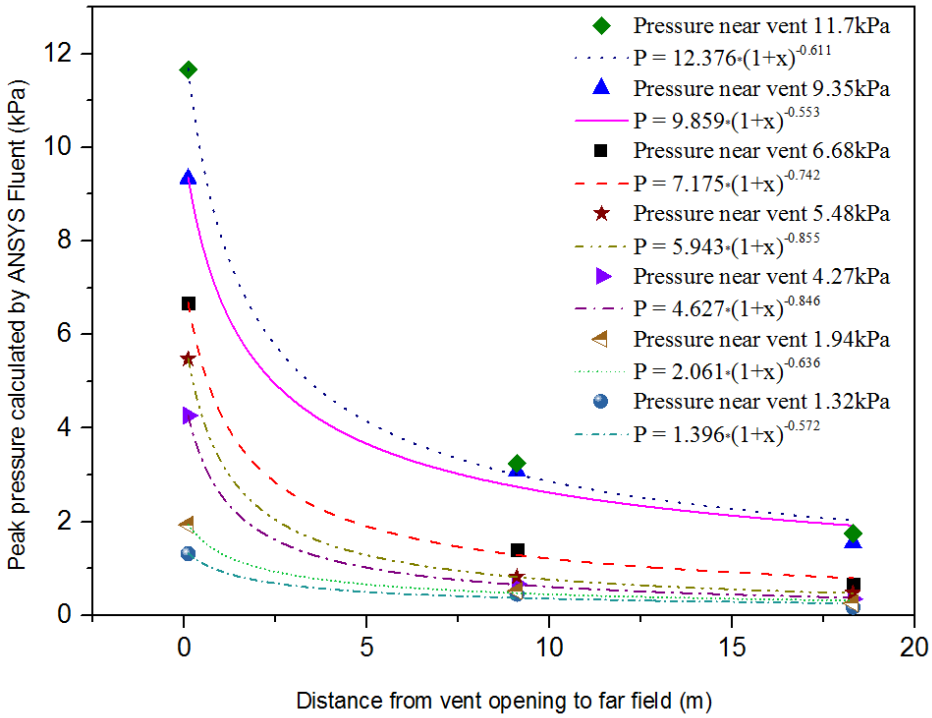

559

560 **Fig. 20 Relation between distances from vent opening and maximum pressures**

561

562 Unlike the simple relation between the pressure and distance from the vent in previous work

563 (Palmer and Tonkin, 1980), more complex relationships between the pressure and distance

564 are found in this study (as seen in Fig. 20). Palmer and Tonkin indicated that external
565 pressure decreases inversely with the increase of distance from the vent opening to far field.
566 Specifically, $P=k\times(d+d_o)^{-1}$, P is the external pressure, k is a constant depending on the fuel
567 properties and vent area size, d_o is the distance from the far end of chamber to vent opening, d
568 is the distance from the vent opening to far field (9m < d <18m). However, it is seen in Fig.
569 20 that the power for each curve has a varying factor from -0.553 to -0.846 instead of the
570 constant -1 in the equation above. In other words, unlike the constant curvature found in
571 (Palmer and Tonkin, 1980), the curvature of external pressure-time curve in far field is
572 varying. The main reason of such difference in authors' findings is that there were only two
573 distances of the total 7 sets of pressure data recorded by Palmer and Tonkin in the
574 experimental study. Therefore only a linear attenuation of peak pressure with distance can be
575 derived. Here using three distance data points (i.e. 21 sets of pressure to distance data)
576 indicates that the peak pressure attenuation with distance does not follow a linear relation, but
577 more like an exponential relation. Nevertheless, 21 sets of data are still limited. More
578 external explosion experiments and CFD simulations are required to derive a less biased
579 correlation, which will be conducted in authors' next paper.

580 **4 Discussion**

581 Based on pre-existing experimental data (Bauwens et al., 2010), this study initially aims to
582 investigate the newly addressed analytical method on pressure prediction from a vented
583 explosion. The peak internal pressures near the vent opening calculated by the analytical
584 approach are proved to be accurate. However, the Taylor instability related constant of Γ_T in
585 the correlations is determined subjectively, the fundamental relations among the constant,
586 vent area, ignition location and gas properties, etc. are not well defined. Moreover, the critical
587 time when the flammable fuel exits the vent needs be determined from the experimental
588 reading, which means the estimation of the critical time for a realistic vented explosion where

589 no experimental data is available has to be done with intelligent assumption, which could be
590 a big challenge because of many factors and uncertainties involved.

591 In terms of the more realistic vented gas explosion, the gas-air mixture cloud can be
592 concentrated as layered in a large enclosure if the gas filling time is long enough. For such
593 realistic scenarios with layered fuel mixtures, the analytical correlations are further utilized to
594 calculate the explosion pressure. Compared with the recorded data in experimental tests on
595 3.9 × 3 × 2.4 m enclosures with different vent areas (Palmer and Tonkin, 1980), it is
596 demonstrated that the analytical method is capable of predicting the peak pressures for the
597 explosion with layered fuel mixture by introducing a new factor. However, the Taylor
598 instability related parameter still needs be determined with some idealised assumption. The
599 comparisons also show that the correlations are incapable of predicting the propagation of the
600 blast wave in the far field.

601 The CFD simulation is therefore introduced to study the realistic vented explosion. More
602 uncertainties are taken into account by using the CFD-based solver FLACS. The gas
603 properties, ignition location, vent area condition, geometry congestion and confinement, etc.
604 are well considered in FLACS explosion simulation. The calculated peak pressures near the
605 vent opening are found in good agreement with the experimental results. However, FLACS
606 simulation underestimates the blast wave propagation in the free air even with the
607 application of the new guideline on far-field pressure prediction (Hansen and Johnson, 2015).
608 The shortcoming of FLACS simulation no able to give good predictions of flame propagation
609 in open space observed in (Ma et al., 2014) is further confirmed in this study.

610 In order to address this problem, especially for far-field pressure prediction initiated from a
611 low turbulent flame source, ANSYS Fluent is utilized. The pressure inlet boundary in
612 ANSYS Fluent is modelled with an UDF file consists of the vent opening pressure-time

output obtained in FLACS. By employing the Navier-Stokes equations (e.g. the Standard k–ε model), accurate grid cell mesh and proper initial condition setups, etc., the pressure-time curves are well predicted in the far field as compared with the testing results. Overall, the peak external pressures predicted by ANSYS Fluent are in satisfactory agreement with 7 sets of experimental data.

5 Conclusion

In this paper, the authors have conducted a comprehensive CFD study on internal and external pressure prediction for a vented explosion with layered gas-air mixture, which is inspired by the inability of analytical correlations to give good predictions of pressure propagations in the far field from the vent opening.

A series of analytical correlations are newly examined based on pre-existing experiments of large-scale vented explosions. Good agreement between the analytical results and experimental observations is achieved in the data comparison. However, the capability of the analytical correlations is restricted on peak internal pressure prediction, while the time history curve is not able to be determined. Furthermore, some parameters of the analytical correlations need be chosen based on idealized assumptions, and the critical time of vent opening is determined from testing data, which is not available for a real vented explosion.

In order to accurately calculate the internal and external pressure of a vented explosion, the authors then offer a thorough CFD simulation procedure by using both FLACS and ANSYS Fluent. The first peak internal pressure inside the enclosure is predicted by using FLACS, which is specialized in turbulent flame modeling. The internal and external explosions near the vent opening simulated from FLACS are then extracted and used as input to ANSYS Fluent for simulating the low turbulent flame propagation in free air. Comparing with the

experimental data, it is found that this approach of combining FLACS and ANSYS Fluent modelling yields accurate predictions of pressure wave propagations in free air from the vent opening.

By taking more external pressure data into consideration, the relation between external pressure and the distance from vent opening to far field is seen differently from previous research's finding (Palmer and Tonkin, 1980). However, the large-scale experiments so far are limited, and more CFD simulations are therefore required to derive reliable relations to predict pressure wave attenuation with distance and estimate the far-field pressures from vented explosions.

Acknowledgement

The authors acknowledge partial financial supports from Australian Research Council project (No. LP130100919) and China National 973 project (No. 2015CB058003) for carrying out this research.

References

Ab Kadir, N.A., Rusli, R., Buang, A., Rahim, N.S.A., 2016. Investigation of the Explosion Behaviour Affected by the Changes of Particle Size. *Procedia Engineer*. 148, 1156-61.

Ansys, I., 2015. CFD. *ICEM CFD theory guide, Ansys inc.*

Arntzen, B.J., 1998. Modelling of turbulence and combustion for simulation of gas explosions in complex geometries.

Baker, W.E., Cox, P., Kulesz, J., Strehlow, R., Westine, P., 2012. *Explosion hazards and evaluation* (Elsevier).

Bao, Q., Fang, Q., Zhang, Y.D., Chen, L., Yang, S.G., Li, Z., 2016. Effects of gas concentration and venting pressure on overpressure transients during vented explosion of methane-air mixtures. *Fuel*. 175, 40-48.

Bauwens, C.R., Chaffee, J., Dorofeev, S., 2008. Experimental and numerical study of methane-air deflagrations in a vented enclosure. *Fire Safety Science*. 9, 1043-54.

Bauwens, C.R., Chaffee, J., Dorofeev, S., 2010. Effect of Ignition Location, Vent Size, and Obstacles on Vented Explosion Overpressures in Propane-Air Mixtures. *Combust Sci Technol*. 182 (11-12), 1915-32.

Bauwens, C.R., Chaffee, J., Dorofeev, S.B., 2011. Vented explosion overpressures from combustion of hydrogen and hydrocarbon mixtures. *Int J Hydrogen Energ*. 36 (3), 2329-36.

Bleyer, A., Taveau, J., Djebaili-Chaumeix, N., Paillard, C.E., Bentaib, A., 2012. Comparison between FLACS explosion simulations and experiments conducted in a PWR Steam Generator casemate scale down with hydrogen gradients. *Nucl Eng Des*. 245, 189-96.

Bradley, D., Mitcheson, A., 1978. The venting of gaseous explosions in spherical vessels. I—Theory. *Combustion and Flame*. 32, 221-36.

Chao, J., Bauwens, C.R., Dorofeev, S.B., 2011. An analysis of peak overpressures in vented gaseous explosions. *P Combust Inst*. 33, 2367-74.

Cooper, M.G., Fairweather, M., Tite, J.P., 1986. On the Mechanisms of Pressure Generation in Vented Explosions. *Combustion and Flame*. 65 (1), 1-14.

Daily-News. 2015. Nigerian president 'shaken and shocked' by gas tank explosion. http://www.dailynewsegypt.com/2015/12/25/nigerian-president-shaken-and-shocked-by-gas-tank-explosion/.

Di Sarli, V., Di Benedetto, A., Russo, G., 2009. Using Large Eddy Simulation for understanding vented gas explosions in the presence of obstacles. *J Hazard Mater*. 169 (1-3), 435-42.

Fakandu, B.M., Andrews, G.E., Phylaktou, H.N., 2015. Vent burst pressure effects on vented gas explosion reduced pressure. *J Loss Prevent Proc*. 36, 431-40.

Fan, B., Jiang, X., Chen, Z., Ye, J., Dong, G., 2005. Investigation on external explosions during venting. *Fire Safety Science*. 8, 1365-74.

Ferguson, C.R., Kirkpatrick, A.T., 2015. *Internal combustion engines: applied thermosciences* (John Wiley & Sons).

Ferrara, G., Willacy, S.K., Phylaktou, H.N., Andrews, G.E., Di Benedetto, A., Salzano, E., Russo, G., 2008. Venting of gas explosion through relief ducts: Interaction between internal and external explosions. *J Hazard Mater*. 155 (1-2), 358-68.

Firehouse. 2008. Lightning Causes Fire at Kansas Fuel Plant. http://www.firehouse.com/news/10503342/lightning-causes-fire-at-kansas-fuel-plant.

Fluent, A., 2009. 12.0 User's guide. *User Inputs for Porous Media*. 6.

Fluent, A., 2012. Ansys Fluent UDF manual. In.: Release.

Forcier, T., Zalosh, R., 2000. External pressures generated by vented gas and dust explosions. *J Loss Prevent Proc*. 13 (3-5), 411-17.

Gexcon. 2015. FLACS v10.4 User's Manual, Norway.

Gordon, S., McBride, B.J., 1994. Computer program for calculation of complex chemical equilibrium compositions and applications. Part 1: Analysis.

Hansen, O.R., Gavelli, F., Ichard, M., Davis, S.G., 2010a. Validation of FLACS against experimental data sets from the model evaluation database for LNG vapor dispersion. *J Loss Prevent Proc*. 23 (6), 857-77.

Hansen, O.R., Hinze, P., Engel, D., Davis, S., 2010b. Using computational fluid dynamics (CFD) for blast wave predictions. *J Loss Prevent Proc*. 23 (6), 885-906.

Hansen, O.R., Johnson, D.M., 2015. Improved far-field blast predictions from fast deflagrations, DDTs and detonations of vapour clouds using FLACS CFD. *J Loss Prevent Proc*. 35, 293-306.

Harrison, A.J., Eyre, J.A., 1987. External Explosions as a Result of Explosion Venting. *Combust Sci Technol*. 52 (1-3), 91-106.

Janes, A., Vignes, A., Dufaud, O., Carson, D., 2014. Experimental investigation of the influence of inert solids on ignition sensitivity of organic powders. *Process Safety and Environmental Protection*. 92 (4), 311-23.

Jiang, X.H., Fan, B.C., Ye, J.F., Dong, G., 2005. Experimental investigations on the external pressure during venting. *J Loss Prevent Proc*. 18 (1), 21-26.

Johnson, D.M., Tomlin, G.B., Walker, D.G., 2015. Detonations and vapor cloud explosions: Why it matters. *J Loss Prevent Proc*. 36, 360-66.

Kuznetsov, M., Friedrich, A., Stern, G., Kotchourko, N., Jallais, S., L'Hostis, B., 2015. Medium-scale experiments on vented hydrogen deflagration. *J Loss Prevent Proc*. 36, 418-30.

Li, J.D., Hernandes, F., Hao, H., Fang, Q., Xiang, H., Li, Z., Zhang, X.H., Li, C., 2017a. Vented methane-air explosion overpressure calculation - a simplified approach based on CFD. *Safety and Environmental Protection*. Under reviewer.

Li, Z., Chen, L., Fang, Q., Hao, H., Zhang, Y.D., Chen, W.S., Xiang, H.B., Bao, Q., 2017b. Study of autoclaved aerated concrete masonry walls under vented gas explosions. *Eng Struct*. 141, 444-60.

Li, Z., Chen, L., Fang, Q., Hao, H., Zhang, Y.D., Xiang, H.B., Chen, W.S., Yang, S.G., Bao, Q., 2017c. Experimental and numerical study of unreinforced clay brick masonry walls subjected to vented gas explosions. *Int J Impact Eng*. 104, 107-26.

Liang, Y.T., Zeng, W., 2010. Numerical study of the effect of water addition on gas explosion. *J Hazard Mater*. 174 (1-3), 386-92.

Luo, C., Zanganeh, J., Moghtaderi, B., 2016. A 3D numerical study on the effects of obstacles on flame propagation in a cylindrical explosion vessel connected to a vented tube. *J Loss Prevent Proc*. 44, 53-61.

Ma, G.W., Li, J.D., Abdel-Jawad, M., 2014. Accuracy improvement in evaluation of gas explosion overpressures in congestions with safety gaps. *J Loss Prevent Proc*. 32, 358-66.

Mercx, W., Van den Berg, A., Mouilleau, Y., 1994. Modelling and experimental research into gas explosions. *Overall report of the MERGE project, CEC contract: STEP-CT-0111 (SSMA).*

Middha, P., Hansen, O.R., 2008. Predicting deflagration to detonation transition in hydrogen explosions. *Process Saf Prog*. 27 (3), 192-204.

Middha, P., Hansen, O.R., Storvik, I.E., 2009. Validation of CFD-model for hydrogen dispersion. *J Loss Prevent Proc*. 22 (6), 1034-38.

Mitu, M., Prodan, M., Giurcan, V., Razus, D., Oancea, D., 2016. Influence of inert gas addition on propagation indices of methane–air deflagrations. *Process Safety and Environmental Protection*. 102, 513-22.

Molkov, V., 1999. Innovative vent sizing technology for gaseous deflagrations. In *Sixth international symposium on fire safety science*.

NFPA-68. 2007. Standard on Explosion Protection by Deflagration Venting, 2013 Edition. *National Fire Protection Association, Quincy, MA*.

NFPA-68. 2013. Standard on Explosion Protection by Deflagration Venting, 2013 Edition. *National Fire Protection Association, Quincy, MA*.

Palmer, K., Tonkin, P., 1980. External pressures caused by venting gas explosions in a large chamber. In *Proceedings of the 3rd International Loss Prevention Symposium*.

Qi, S., Du, Y., Wang, S.M., Zhou, Y., Li, G.Q., 2016. The effect of vent size and concentration in vented gasoline-air explosions. *J Loss Prevent Proc*. 44, 88-94.

Rocourt, X., Awamat, S., Sochet, I., Jallais, S., 2014. Vented hydrogen-air deflagration in a small enclosed volume. *Int J Hydrogen Energ*. 39 (35), 20462-66.

Schildknecht, M., Geiger, W., 1983. Explosion development in unconfined and partially coinfined ethylene/air mixtures due to jet ignition. In *Proceedings Fourth International Symposium on Loss Prevention and Safety Promotion in the Process Industries*. D30.

Solberg, D., Pappas, J., Skramstad, E., 1980. Experimental investigations on flame acceleration and pressure rise phenomena in large scale vented gas explosions. In *Proceedings of 3rd International Symposium on Loss Prevention and Safety Promotion in Process Industries, Basle*. 16.

Strehlow, R.A., 1979. The blast wave from Deflagrative explosions, an acoustic approach. In.: DTIC Document.

Tamanini, F., 1993. Characterization of mixture reactivity in vented explosions. In *14th International Colloquium on the Dynamics of Explosions and Reactive Systems*. 1-6.

Tamanini, F., 2001. Scaling parameters for vented gas and dust explosions. *J Loss Prevent Proc*. 14 (6), 455-61.

Tamanini, F., 2002. Dust explosion vent sizing - Current methods and future developments. *J Phys Iv*. 12 (Pr7), 31-44.

Thomas, J.K., Goodrich, M.L., Duran, R.J., 2013. Propagation of a vapor cloud detonation from a congested area into an uncongested area: Demonstration test and impact on blast load prediction. *Process Saf Prog*. 32 (2), 199-206.

TNA, T.N.A., 2011. Explosion at oil depot in Russia's Far East kills three. http://en.trend.az/world/other/1883483.html.

Tomlin, G., Johnson, D., 2013. A large scale study of the venting of confined explosions into unobstructed and congested flammable vapour clouds. In *7th International Seminar on Fire and Explosion Hazards, Providence, RI*.

Tomlin, G., Johnson, D.M., Cronin, P., Phylaktou, H.N., Andrews, G.E., 2015. The effect of vent size and congestion in large-scale vented natural gas/air explosions. *J Loss Prevent Proc*. 35, 169-81.

Tulach, A., Mynarz, M., Kozubkova, M., 2015. CFD simulation of vented explosion and turbulent flame propagation. *Epj Web Conf*. 92.

Van den Berg, A., 1985. The multi-energy method: a framework for vapour cloud explosion blast prediction. *J Hazard Mater*. 12 (1), 1-10.

Van Wingerden, C., 1989. On the venting of large-scale methane–air explosions. In *6th International Symposium of Loss Prevention and Safety Promotion in the Process Industries*. 19-22.

Highlights

- A series of analytical correlations are newly examined based on pre-existing experiments of large-scale vented explosions
- The inability of analytical correlations in the far-field pressure prediction inspires the CFD study on external explosion simulation.
- Large-scale vented gas explosion, which has rarely been numerically studied and indexed in literature, has been investigated.
- A combined CFD modelling procedure is proposed to predict the internal and external pressures separately by using FLACS and Fluent.